International Journal of Earth, Energy and Environmental Sciences
ISSN: 2517-942X
Vol:7, No:10, 2013

Remote Sensing, GIS, and AHP for Assessing Physical Vulnerability to Tsunami Hazard

Abu Bakar Sambah, Fusanori Miura

***Abstract*—**Remote sensing image processing, spatial data analysis through GIS approach, and analytical hierarchy process were introduced in this study for assessing the vulnerability area and inundation area due to tsunami hazard in the area of Rikuzentakata, Iwate Prefecture, Japan. Appropriate input parameters were derived from GSI DEM data, ALOS AVNIR-2, and field data. We used the parameters of elevation, slope, shoreline distance, and vegetation density. Five classes of vulnerability were defined and weighted via pairwise comparison matrix. The assessment results described that 14.35km^2 of the study area was under tsunami vulnerability zone. Inundation areas are those of high and slightly high vulnerability. The farthest area reached by a tsunami was about 7.50km from the shoreline and shows that rivers act as flooding strips that transport tsunami waves into the hinterland. This study can be used for determining a priority for land-use planning in the scope of tsunami hazard risk management.

***Keywords*—**AHP, GIS, remote sensing, tsunami vulnerability.

I. Introduction

NATURAL hazards are natural phenomena whose occurrence is almost impossible to reduce. We only can minimize the impact of these events by performing an initial assessment in order to map the vulnerable areas. Vulnerability is one of the parameters used to determine disaster risk, together with hazard probability, exposure, and capacity measures [1], [2].

The development of remote sensing technology enables the use of satellite imagery for mapping the damage area due to a disaster and for assessing the vulnerable areas. Satellite images have the advantage of observing large areas in both high spatial and high temporal resolution [3]-[5]. Moreover, a geographical information system (GIS) is useful for analyzing spatial data due to disaster mitigation planning.

Spatial data analysis via spatial multicriteria analysis helps prioritize the decision-making process using georeference data to manage different spatial information and combine them for better decision making. Spatial multi-criteria analysis uses information on both the criterion values and the geographical positions of alternatives in addition to the decision maker's preferences with respect to a set of evaluation parameters [6], [7].

Abu Bakar Sambah (Ph.D student) is with the Graduate School of Science and Engineering, Yamaguchi University, Japan, and Fisheries and Marine Science Faculty, Brawijaya University, Indonesia (corresponding author; phone: +8190 6404 1707, e-mail: absambah@yahoo.com, r501wf@yamaguchi-u.ac.jp).

Fusanori Miura is with the Graduate School of Science and Engineering, Yamaguchi University, Japan, (e-mail: miura@yamaguchi-u.ac.jp).

Remote sensing data of moderate-resolution optical satellite images has been used to identify the inundation area and to assess the vulnerability and risk in coastal area. GIS is also applied to evaluate the strategy for coastal vegetation belts against tsunami risk and to analyze tsunami risk using a multiscenario approach [8]-[11].

A previous study analyzed vulnerability using remote sensing data and integrated analysis using the GIS with regard to physical infrastructure (i.e., buildings) and identified the inundation area based on contours and the highest recorded tsunami event related to building vulnerability and human vulnerability [5], [12]-[14]. Another study developed the Papathoma Tsunami Vulnerability Assessment (PTVA) to provide first-order assessments of building vulnerability to tsunami [15], [13]. The use of multi-criteria analysis and the analytic hierarchy process (AHP) was introduced in vulnerability mapping and assessing tsunami vulnerability, which have been done at the regional scale using ASTER imagery and digital elevation models of 3 arc-seconds SRTM-version 3 data [16], [17].

In this study, we tried to apply input parameters of elevation, slope, shoreline distance, and vegetation density and analyze them via AHP and GIS in terms of spatial multi criteria to map the tsunami vulnerability area. This study was applied in the area of Rikuzentakata in Iwate Prefecture, Japan (see Fig. 1). The general steps adopted in this study are shown in Fig. 2.

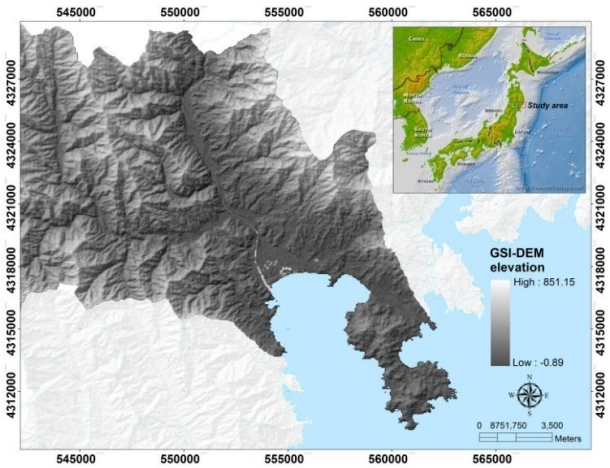

Fig. 1 Study area

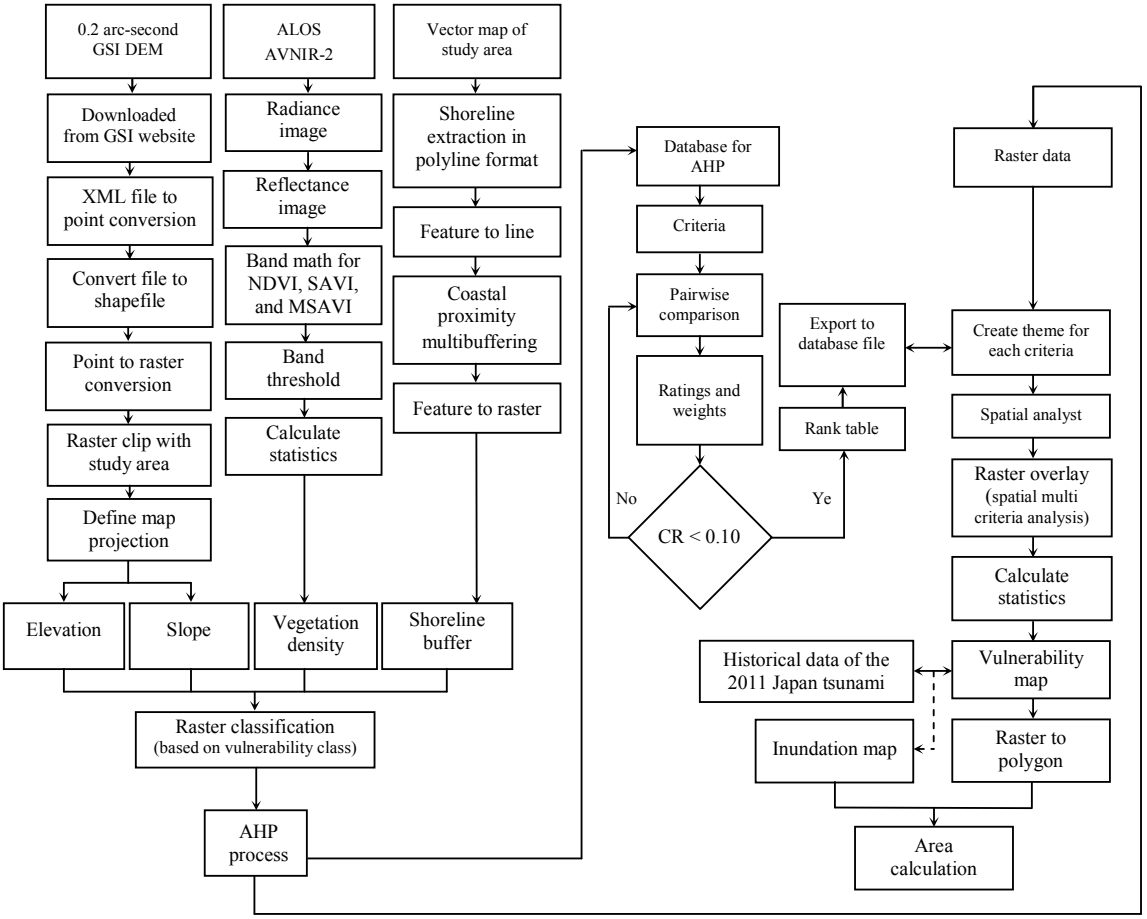

GSI : Japan's Geographical Survey Institute, DEM : Digital Elevation Model, XML : Extensible Markup Language, ALOS : Advanced Land Observation Satellite, AVNIR-2 : the Advanced Visible And Near Infrared Radiometer type 2, NDVI : Normalized Difference Vegetation Index, SAVI : Soil-Adjusted Vegetation Index, MSAVI : a Modified Soil-Adjusted Vegetation Index, AHP : Analytical Hierarchy Process, CR : Consistency Ratio.

Fig. 2 Framework of the study

The parameters of elevation and slope were extracted from a digital elevation model (DEM) obtained from the Geospatial Information Authority of Japan (hereafter referred to as GSI DEM), while the vegetation density is extracted from an ALOS AVNIR-2 image. We measured shoreline distance from a vector map of the study area.

II. Surface Analysis for Spatial Data

A. Elevation

We created a digital elevation model from elevation data obtained from GSI. GSI DEM was downloaded from http://fgd.gsi.go.jp/download/GsiDLSelFileServlet. We used 5m mesh elevation data (0.2 seconds). The 5m mesh elevation was created based on the airborne laser survey of the center point grid (mesh) and the data obtained by the photogrammetry with a longitude difference at the surface separated by an interval of 0.2 seconds latitude difference. The height accuracy of the 5m mesh elevation from the airborne laser is 0.3m and the standard deviation of the elevation point from the photogrammetry is 0.7m. The data was in JPGIS format. We needed several JPGIS data that covered our study area.

We converted each JPGIS data to shapefile in point format using base map viewer converter software version 3.10 (FGDV) provided by GSI. The shapefile data were then combined using the merge function of ArcGIS 10 based on the area of study, and finally, we converted this point format to raster for creating the digital elevation model. The steps are shown in Fig. 3.

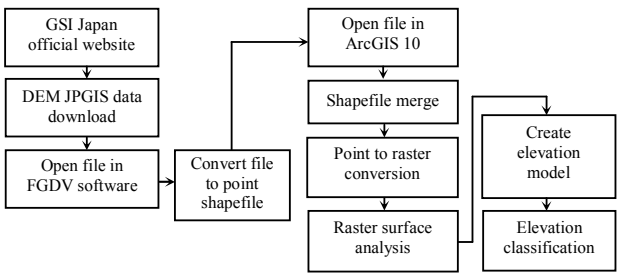

Fig. 3 Elevation data process

B. Slope

The slope is the rate of maximum change in *z*-value from each cell of the image. The use of a *z*-value is essential for correct slope calculations when the surface *z* units are expressed in units different from the ground *x*, *y* units. The range of values in the output depends on the type of measurement units. We created a slope map using the surface analyst tools of the ArcGIS 10 software using the third-order finite-difference method [18].

C. Shoreline Distance

We created shoreline in polyline file for buffering the distance from shoreline to the land. We calculated the distance using a multiring buffer under the proximity tool in the ArcGIS 10 software. The distance is based on the historical report of the maximum run-up in the area of study. Equation (1) used for shoreline distance buffering [10].

$$\mathrm{Log}X_{max} = \log 1400 + \tfrac{3}{4}\log\left(\tfrac{Y_0}{10}\right) \quad (1)$$

in which X_{max} is the maximum reach of the tsunami over land, and Y_0 is the tsunami height at the coast.

The maximum run-up of the tsunami in the study area due to the 2011 Tohoku earthquake was 18.8m. Based on the algorithm above, five classes of distance buffers were used in order to create a tsunami vulnerability map. It describes that 9.40m to 11.28m of run-up can reach a distance of 1,289.14m from the coastline, 11.28m to 13.16m of run-up can reach 1,643.89m, 13.16m to 15.04m of run-up can reach 2,019m, 15.04m to 16.92m of run-up can reach 2,412.45m, and 16.92m to 18.80m of run-up can reach more than 2,412.45m.

We classified elevation, slope, and shoreline distance into five classes of vulnerability using the Jenks natural breaks method. This classification method identifies breaks in the ordered distribution of values that minimizes within class sum of squared. We classified elevation, slope, and shoreline distance based on the values described in Table I. The tsunami vulnerability map based on elevation is shown in Fig. 4, one based on slope is shown in Fig. 5, and one based on shoreline distance is shown in Fig. 6.

TABLE I
TSUNAMI VULNERABILITY CLASSES BASED ON ELEVATION, SLOPE, AND SHORELINE DISTANCE

Elevation (meter)[19]	Slope (%) [20]	Distance (meter)	Vulnerability class
< 5	0 – 2	0 – 1,289.14	High
5 –10	2 – 6	1,289.14 – 1,643.89	Slightly high
10 – 15	6 – 13	1,643.89 – 2,019	Medium
15 – 20	13 – 20	2,019 – 2,412.45	Slightly low
> 20	> 20	> 2,412.45	Low

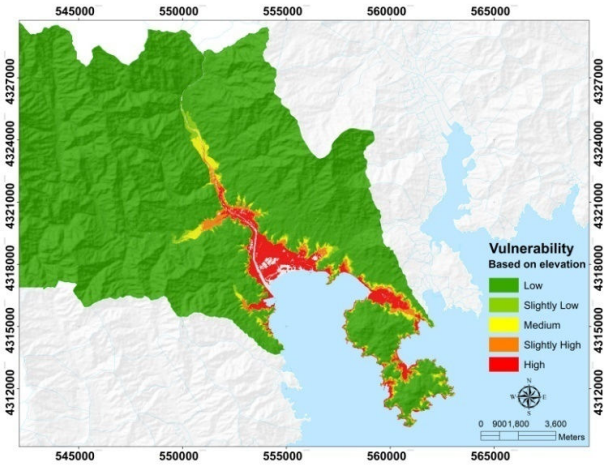

Fig. 4 Vulnerability map based on elevation

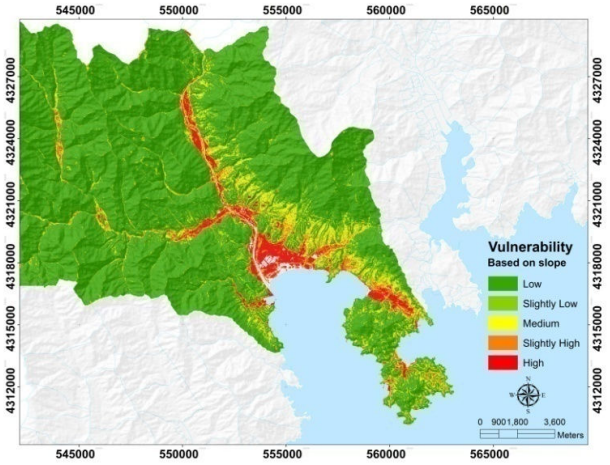

Fig. 5 Vulnerability map based on slope

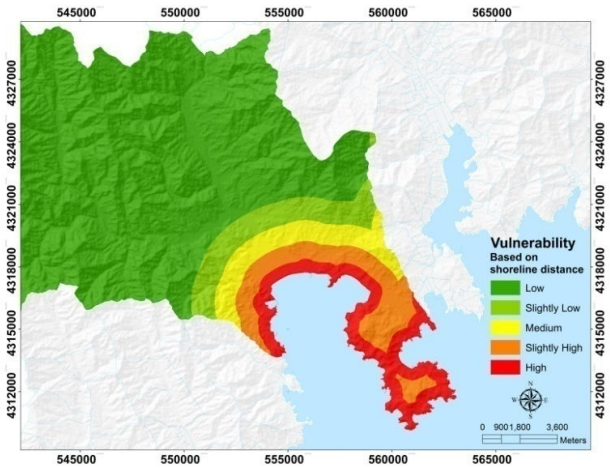

Fig. 6 Vulnerability map based on shoreline distance

TABLE II
RESCALING GAINS AND BIASES USED FOR DN TO SPECTRAL RADIANCE CONVERSION FOR ALOS AVNIR-2

Band	Grescale	Brescale
1	0.5888	0
2	0.5730	0
3	0.5020	0
4	0.8350	0

III. ALOS AVNIR-2 PROCESSING

ALOS AVNIR-2 was used to generate vegetation density. We calculated normalized difference vegetation index (NDVI), soil-adjusted vegetation index (SAVI), and a modified soil-adjusted vegetation index (MSAVI) instead of vegetation density. The digital numbers (DNs) of ALOS AVNIR-2 were converted to reflectance values before generating the synthetic NDVI and SAVI images [21], [22]. The steps to create vegetation density map are as follows:

A. DN to Radiance Conversion

Equation (2) describes the algorithm for DN to radiance conversion [23].

$$L_\lambda = G_{rescale} \times QCAL + B_{rescale} \quad (2)$$

in which L_λ is the spectral radiance at the sensor's aperture ($W/m^2/sr/\mu m$), $G_{rescale}$ is the rescaled gain, QCAL is the DN, and $B_{rescale}$ is the rescaled bias. Table II describes rescaled gains and biases for ALOS AVNIR-2.

B. Radiance to Reflectance Conversion

Equation (3) describes the algorithm for radiance to reflectance conversion [24].

$$\rho_\lambda = \pi \times L_\lambda \times d^2 / ESUN_\lambda \times \cos\theta_s \quad (3)$$

in which ρ_λ is the unitless planetary reflectance, L_λ is the spectral radiance at the sensor's aperture, d^2 is the Earth-sun distance in astronomical units from a nautical handbook, $ESUN_\lambda$ is the mean solar exoatmospheric irradiances, and θ_s is the solar zenith angle in degrees.

C. NDVI, SAVI, and MSAVI Calculation

NDVI is a measure of the difference in reflectance between these wavelength ranges that takes values between −1 and 1, with values > 0.5 indicating dense vegetation and values < 0 indicating no vegetation including water. Equation (4) was used for NDVI calculation [25].

$$NDVI = \frac{(NIR - VIS)}{(NIR + VIS)} \quad (4)$$

in which *NIR* is near an infrared band and *VIS* is a visible band of red band of ALOS AVNIR-2. Band 3 is red, and band 4 is *NIR*. Moreover, SAVI is one of the algorithms developed to generate vegetation index by eliminating soil factor [26]. Although the SAVI model is not significant in the intraclass analysis, in the similar spectral space, this model presents a reasonable performance in the characterization of forested and nonforested areas [22]. SAVI was developed to minimize soil-brightness, including shadow, influences found in the NDVI by accounting for first-order soil-vegetation spectral interactions as in (5) [27].

$$SAVI = \frac{(NIR - R)}{(NIR + R + L)} \times (1 + L) \quad (5)$$

in which *NIR* is the near infrared band, *R* is the red band, and *L* is the soil calibration factor. $L = 0.5$ [28].

A correction factor (L) was used to minimize the secondary backscattering effect of canopy-transmitted soil background reflected radiation. The L value of 1 was optimal in semiarid environments.

MSAVI is a modified version of SAVI, which replaces the constant soil adjustment factor, L, with a self-adjusting L. SAVI uses a manual adjustment L, while MSAVI uses a self-adjusting L. The former requires prior knowledge about vegetation densities in order to use an optimal L value in the SAVI equation, while the latter automatically adjusts its L values to optimal [29]. Equation (6) describes the algorithm for MSAVI calculation.

$$MSAVI = \frac{1}{2}\left(2B4 + 1 - \sqrt{(2B4+1)^2 - 8(B4 - B3)}\right) \quad (6)$$

The regression between NDVI and MSAVI values describes that R^2 was 0.9658 (see Fig. 7). We used MSAVI for vegetation density mapping because it provides a vegetation index where soil factors are eliminated. MSAVI values ranged between −0.058 to 0.537. We classified MSAVI values into five classes of vulnerability for generating a tsunami vulnerability map based on vegetation density using the Jenks natural breaks method. The classification was based on the maximum and minimum values of MSAVI as shown in Table III.

TABLE III
TSUNAMI VULNERABILITY CLASSES BASED ON VEGETATION DENSITY

Vegetation density	Vegetation index	Vulnerability class
Rarely	(−)0.05761 – 0.046204	High
Slightly rarely	0.046204 – 0.091981	Slightly high
Medium	0.091981 – 0.133113	Medium
Slightly high	0.133113 – 0.178984	Slightly low
High	0.178984 – 0.537292	Low

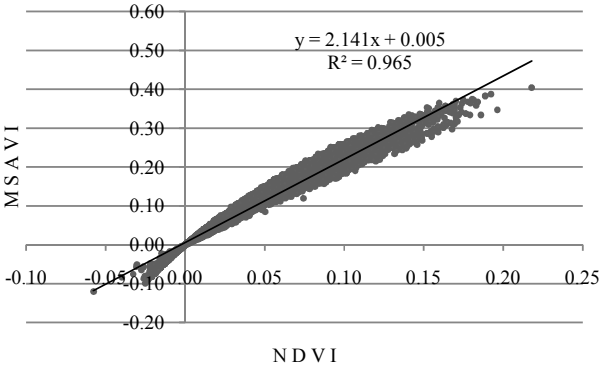

Fig. 7 Scatterplot of NDVI and MSAVI values

A vulnerability map based on vegetation density, as shown in Fig. 8, described that most of high-vulnerability areas were found in the coastal areas of Rikuzentakata and indicated as bare areas.

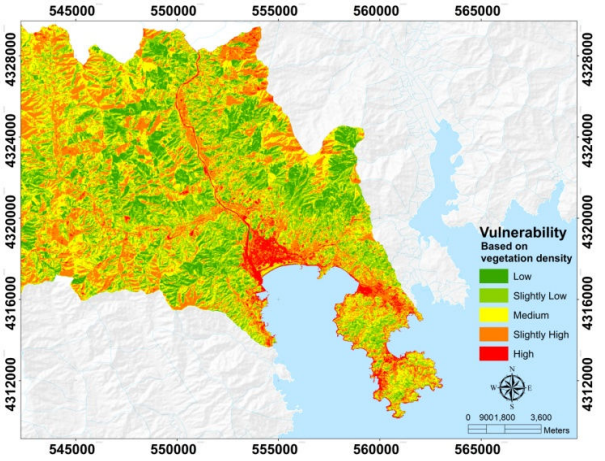

Fig. 8 Vulnerability map based on vegetation density

IV. GIS and AHP for Vulnerability Mapping

We used cell-based modeling in spatial analysis to determine the vulnerability area due to tsunami hazard. Cells are classified into five classes of vulnerability in the numbers of 1, 2, 3, 4, and 5, which represent low, slightly low, medium, slightly high, and high vulnerability classes.

We then overlay the entire parameter of tsunami vulnerability by using a weighting and scoring system. Weighting is based on the dominant influences of these parameters in determining the class of tsunami vulnerability. For this step, we applied AHP.

AHP helps in creating a scaled set of preferences and describing the importance of each parameter relative to other parameters through pairwise comparisons [30]-[32]. We established priorities among the parameters of the hierarchy by creating a series of judgments based on pairwise comparisons of the parameters, where a number from 1 to 9 is used in the matrix cell value for scoring the importance of each parameter. Table IV describes the Saaty nine-point comparison scale. This number depends on the relative importance of each parameter.

TABLE IV
The Saaty Nine-Point Comparison Scale [34]

Score	Definition	Explanation
1	Equal importance	Two parameters contribute equally to the objective.
3	Weak importance of one over another	The judgment is to favor one parameter over another, but it is not conclusive.
5	Essential or strong importance	The judgment is to strongly favor one parameter over another.
7	Demonstrated importance	Conclusive judgment as to the importance of one parameter over another.
9	Absolute importance	The judgment in favor of one parameter over another is of the highest possible order of affirmation.
2, 4, 6, 8	Intermediate values between the two adjacent judgments	Compromise is needed.

TABLE V
Pairwise Comparison

	Elevation	Slope	Shoreline distance	Vegetation density
Elevation	1	2	3	3
Slope	1/2	1	2	2 1/2
Shoreline distance	1/3	1/2	1	3
Vegetation density	1/3	2/5	1/3	1

The relative weights of each parameter will be produced via pairwise comparison as shown on Table V. We calculated hierarchical interactions based on the respective importance of each parameter by assessing the numerical score. These values are generated by the subjective determination of the investigator in determining the importance of each factor [32], [33].

We calculated the eigenvector based on the pairwise comparison matrix in five iterations. The normalized principal eigenvector in five iterations describes that elevation has the highest weight (45.94%), followed by slope (25.53%), shoreline distance (16.71%), and vegetation density (11.81%), as shown in Fig. 9.

$$\begin{array}{l} \\ \text{Elevation} \\ \text{Slope} \\ \text{Shoreline distance} \\ \text{Vegetation density} \end{array} \begin{array}{c} \text{Normalized matrix} \\ \begin{pmatrix} 0.4615 & 0.5129 & 0.4737 & 0.3158 \\ 0.2308 & 0.2564 & 0.3148 & 0.2632 \\ 0.1539 & 0.1282 & 0.1579 & 0.3158 \\ 0.1539 & 0.1026 & 0.0526 & 0.1053 \end{pmatrix} \end{array}$$

$$1^{st}\ \text{iteration} \begin{pmatrix} 0.4528 & 0.4613 & 0.4720 & 0.4635 \\ 0.2548 & 0.2516 & 0.2540 & 0.2678 \\ 0.1735 & 0.1644 & 0.1549 & 0.1654 \\ 0.1190 & 0.1227 & 0.1191 & 0.1033 \end{pmatrix} \begin{pmatrix} 46.24\% \\ 25.70\% \\ 16.46\% \\ 11.60\% \end{pmatrix}$$

$$5^{th}\ \text{iteration} \begin{pmatrix} 0.4595 & 0.4595 & 0.4595 & 0.4595 \\ 0.2554 & 0.2554 & 0.2554 & 0.2554 \\ 0.1671 & 0.1671 & 0.1671 & 0.1671 \\ 0.1181 & 0.1181 & 0.1181 & 0.1181 \end{pmatrix} \begin{pmatrix} 45.94\% \\ 25.53\% \\ 16.71\% \\ 11.81\% \end{pmatrix}$$

Fig. 9 Normalized eigenvector calculation

TABLE VI
RANDOM CONSISTENCY INDEX

Matrix size	1	2	3	4	5	6	7	8
Random CI	0	0	0.58	0.90	1.12	1.24	1.32	1.41

AHP tolerates inconsistency by providing a measure of inconsistency assessment, which is shown by consistency ratio (CR). An acceptable CR is less than or equal to 10%, although in some cases a consistency ratio greater than 10% can be considered acceptable [35]. CR is defined as the ratio between the consistency index (CI) and random consistency index (RI). CR indicates the probability that the matrix judgments were randomly generated [30]. Equation (7) describes the algorithm for CR and CI calculation.

$$CR = \frac{CI}{RI}, and\ CI = \frac{(\lambda_{max} - N)}{(N - 1)} \quad (7)$$

in which λ_{max} represents the largest eigenvalue and N is the size of the the comparison matrix. In this study, $N = 4$.

λ_{max} is calculated from the sum of all parameters and is multiplied by its eigenvector. The *RI* is based on the random consistency index as shown in Table VI. We used an *RI* of 0.90 for four parameters. Five iterations of normalized matrix in Fig. 9 produces the value of *CI* was 0.057 and *CR* was 6.4%.

In order to create the vulnerability map, we calculated each raster cell of the parameter to its weight. A weighted linear combination is very straightforward in a raster GIS, and factors are combined by applying a weight value to each, followed by a summation of the results [36]. We used a raster calculator in map algebra menu using the spatial analyst tools of ArcGIS 10 to generate vulnerability mapping by applying (8). The tsunami vulnerability map in the Rikuzentakata area as result of this calculation is shown in Fig. 10.

$$\sum (W_i \cdot X_i) \quad (8)$$

in which Wi is the weight values of the parameter i and Xi is the potential rating of the factor.

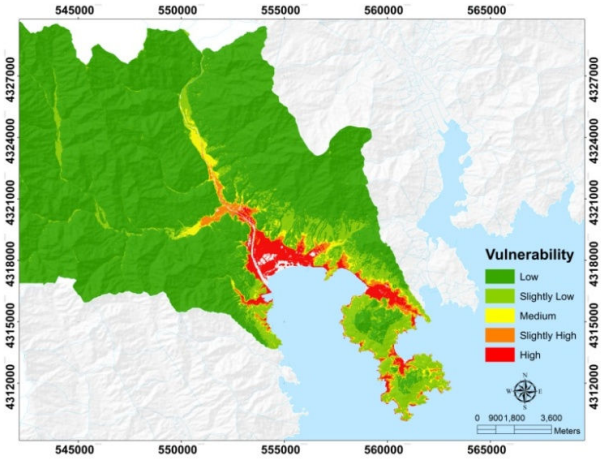

Fig. 10 Tsunami vulnerability map of Rikuzentakata

TABLE VII
VULNERABILITY CLASSIFICATION

Vulnerability classes	Vulnerability (grid) value	Vulnerability index	Area (km^2)	(%)
Low	1 − 1.8	1	117.88	49.55
Slightly low	1.8 − 2.6	2	67.16	28.23
Medium	2.6 − 3.4	3	38.52	16.19
Slightly high	3.4 − 4.2	4	10.05	4.22
High	4.2 − 5	5	4.30	1.81

The vulnerability class is shown in Table VII. We calculated the statistics of the vulnerability map, which shows that the vulnerability index of 822,634.39 grid cells ranged between 1 to 5, with a standard deviation of 0.766.

We compared our results with the historical data of the impact of the 2011 Japan tsunami from GSI (see Fig. 11) and the 2011 Earthquake Tsunami Joint Survey Group. The comparison describes that most of inundation areas are areas of high and slightly high vulnerability.

The inundation area, as result of our study, was 14.35km^2 as shown in Fig. 12, while GSI reported that the inundation area in Rikuzentakata because of the 2011 Japan tsunami was 13 km^2.

The maximum run-up in Rikuzentakata based on the 2011 Earthquake Tsunami Joint Survey Group was 18.81m and found in the area of Yamanawashiro (in the latitude of 39.021 and longitude of 141.647). This area was identified as a bare area and in the class of slightly high vulnerability. The farthest area reached by the tsunami during the 2011 Japan tsunami was about 7.50km from the shoreline, with an inundation height of 11.08m (in the latitude of 39.063 and longitude of 141.589). This area was close to the river and identified in the class of slightly high vulnerability.

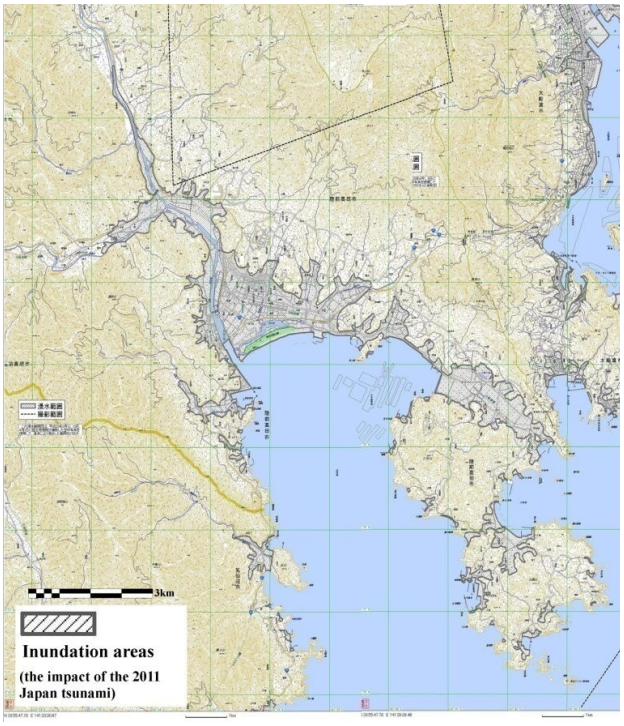

Fig. 11 Map of the impact of the 2011 Japan tsunami in Rikuzentakata, published by GSI [37]

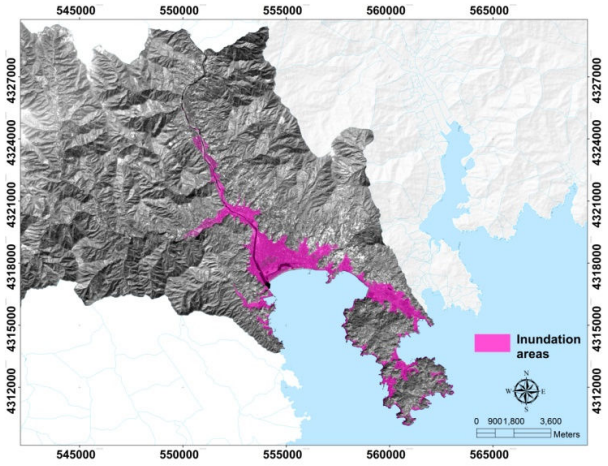

Fig. 12 Map of possible inundation areas in Rikuzentakata

In addition, Table VIII describes the value of some data that were used as the parameters in this study. Based on the vulnerability class that is described in the previous section (see Tables I and III), in general, these values are included in the class of high vulnerability.

V. Discussion

Vulnerability describes the potential area that can be damaged by natural hazards. Vulnerability class could be based on a physical parameter, such as elevation, slope, shoreline distance, and vegetation density. Moreover, inundation can be defined as the result of a tsunami traveling a long distance inland and is a horizontal measurement of the path of the tsunami. The analysis of satellite remote sensing data, elevation data, and survey data followed by multi-criteria analysis through AHP and raster overlay in GIS processing can be used as the basic information for vulnerability mapping and inundation assessment due to tsunami hazard. The use of the AHP method helps in the analysis of spatial multi-criteria where all the parameters used in this study were calculated based on their weight factors to create a vulnerability map.

This study is a first attempt to assess tsunami vulnerability by using the parameter of MSAVI instead of vegetation index mapping besides elevation, slope, and shoreline distance and applying AHP methods combined with raster overlay through GIS processing in the Rikuzentakata area. A simple method for inundation prediction that was performed in this study can be a valuable step for carrying out a preliminary tsunami vulnerability mapping and impact assessment when the high resolution of digital elevation model data and detailed topographic data are not available.

Remote sensing can be effective for deriving information about the input parameters for tsunami vulnerability mapping and impact assessment. For the large area of study, several indicators of vulnerability can be obtained using a middle-resolution satellite. ALOS AVNIR-2 is useful for preparing the input parameters of vegetation density. Although obtaining the digital elevation model from GSI DEM needs some processing, it was very useful to derive information about the digital elevation model in high spatial resolution, especially for areas of study around Japan. GIS is a powerful tool for processing and combining spatial data of each parameter and analyzing the result of AHP in order to generate a vulnerability map.

In this research, five classes of vulnerability were used. The tsunami vulnerability map describes that 117.88km^2 of the area was in low vulnerability, 67.16 km^2 was in slightly low vulnerability, 38.52 km^2 was in medium vulnerability, 10.05 km^2 was in slightly high vulnerability, and 4.30 km^2 was in high vulnerability. The high-vulnerability areas were mostly found in the coastal areas of the sloping coast type. Inundation areas were predicted in areas identified as high-vulnerability and rather-high-vulnerability areas. In addition, we assumed that vegetation may play an important role as tsunami barriers to reduce the impact of tsunami destruction, and a river or another water channel can act as a flooding strip that transports inundation into the hinterland. The run-up of the tsunami comes up to the hinterland not only through the flat surface of the area but also because of the river. This is shown in the inundation map, which described that the farthest area reached by tsunami was about 7.50km from the shoreline, and this area was close to the river. The tsunami vulnerability map and inundation map generated in this study can be used for determining the priority for land-use planning related to tsunami hazard risk management.

In this study, we introduced the combination analysis of digital elevation data, middle-resolution of satellite images, tsunami historical data, AHP, and spatial multi-criteria

processing via GIS to provide a tsunami vulnerability map and inundation map. As a preliminary study, we calculated the reflectance value of an ALOS AVNIR-2 image before and after the 2011 Japan tsunami. In the next study, we will analyze satellite images to assess the characteristics of the inundation area by comparing the before and after images of the disaster event.

TABLE VIII
PARAMETERS VALUE IN THE AREA OF INUNDATION

Parameters	Average value
Eelevation (meter)	4.425
Slope (%)	8.052
NDVI	0.089
SAVI	0.048
MSAVI	0.040
ALOS AVNIR-2 reflectance (18 March 2009)	0.244
ALOS AVNIR-2 reflectance (14 March 2011)	0.137

VI. CONCLUSION

GIS application followed by satellite image processing and AHP method in multi-criteria analysis is useful for tsunami vulnerability mapping and impact assessment. GIS indicate the vulnerability area due to tsunami and describe the possibility areas that could be affected by tsunami waves. In the scope of disaster mitigation planning, this study can be used for the evacuation and reconstruction plan due to tsunami hazards. In this study, we applied four parameters in order to create a tsunami vulnerability map and to map the inundation areas in the area of Rikuzentakata, Iwate Prefecture, Japan. The vulnerability map showed that most of the coastal areas are vulnerable to tsunami hazard. The inundation pattern, as the result of this study, showed similarities to the inundation areas of the 2011 Tohoku earthquake in the area of Rikuzentakata. This study used high resolution of DEM for the input parameters of elevation and slope. We also calculated MSAVI for the parameter of vegetation index.

In the case of data limitation, the use of other DEM is needed. By adding other parameters, such as coastal type, relative direction of tsunami, and coastal bathymetry, better tsunami vulnerability mapping can be done. We recommend to the user to be aware of the assumptions made as well as the limitations within this study. Environmental vulnerability assessment as well as social and economic data can be applied for further works.

In conclusion, the use of remote sensing data followed by AHP processing and spatial multi-criteria analysis via the GIS approach can be applied not only for tsunami vulnerability mapping but also for the assessment of the areas that could be affected by tsunami hazard.

ACKNOWLEDGMENT

GIS DEM is a product of GSI Japan. The authors would like to thank the Japan Aerospace Exploration Agency (JAXA) for the ALOS images and GSI for providing DEM data and vector maps of the study area. Authors are thankful to the 2011 Tohoku Earthquake Tsunami Joint Survey for the survey data in the study area. The first author also thanks the Indonesia Directorate General for Higher Education and Yamaguchi University for scholarship support and research support.

REFERENCES

[1] M. Pelling, *The vulnerability of Cities: Natural Disasters and Social Resilience*, Earthscan Publication, London, 2003.
[2] C. Bollin, C. Cardenas, H. Hahn, and K. S. Vasta, *Disaster Risk Management by Communities and Local Governments*, Inter-American Development Bank, Washinton DC, 2003.
[3] Karen E. Joyce, Kim C. Wright, Sergey V. Samsonov and Vincent G. Ambrosia, *Remote Sensing and The Disaster Management Cycle*, Advances in Geoscience and Remote Sensing, Gary Jedlovec (Ed.), ISBN:978-953-307-005-6, InTech Published, 2009.
[4] F. Yamazaki, Y. Yano, and M. Matsuoka, "Visual damage interpretation of buildings in Bam city using Quickbird images following the 2003 Bam, Iran earthquake," *Earthquake Spectra*, vol. 21, no. S1, pp. S329−S336, 2005.
[5] F. Yamazaki and M. Matsuoka, "Remote sensing technology in post-disaster damage assessment," *Journal of Earthquakes and Tsunamis*, *World Scientific Publishing Company*, vol. 1, no. 3, 2007, pp. 193−210.
[6] S. J. Carver, "Integrating multi-criteria evaluation with geographical information systems," *International Journal of Geographical Information Systems*, vol. 5, no. 3, pp. 321−339, 1991.
[7] P. Jankowski, "Integrating geographic information systems and multiple criteria decision making methods," *International Journal of Geographic Information System*, vol. 9, no. 3, pp. 251−273, 1995.
[8] S. Eckert, R. Jelinek, G. Zeug, and E. Krausmann, "Remote sensing-based assessment of tsunami vulnerability and risk in Alexandria, Egypt," *Applied Geography*, vol. 32, no. 2, pp. 714−723, 2012.
[9] R. S. Mahendra, P. C. Mohanty, H. Bisoyi, T. S. Kumar, and S. Nayak, "Assessment and management of coastal multi-hazard vulnerability along the Cuddalore Villupuram, east coast of India using geospatial techniques," *Ocean & Coastal Management*, vol. 54, no. 4, pp. 302−311, 2011.
[10] T. P. Sinaga, N. Adhi, Yang-Won Lee, and S. Yongcheol, "GIS mapping of tsunami vulnerability: case study of the Jembrana Regency in Bali, Indonesia," *KSCE Journal of Civil Engineering*, vol. 15, no. 3, pp. 537−543, 2011.
[11] F. Usman and K. Murakami, "Preliminary evaluation for strategy on coastal vegetation belt againt tsunami hazard in Pacitan, Indonesia," *European Journal of Scientific Research*, vol. 63, no. 4, pp. 530−542, 2011.
[12] G. Strunz, J. Post, K. Zosseder, S. Wegscheider, M. Muck, T. Riedlinger, H. Mehl, S. Dech, J. Birkmann, N. Gebert, H. Harjono, H. Z. Anwar, Sumaryono, R. M. Khomarudin, and A. Muhari, "Tsunami risk assessment in Indonesia," *Natural Hazards and Earth System Science*, vol. 11, pp. 67−82, 2011.
[13] M. Papathoma and D. Dominey-Howes, "Tsunami vulnerability assessment and its implications for coastal hazard analysis and disaster management planning, Gulf of Corinth, Greece," *Natural Hazards and Earth System Sciences*, vol. 3, no. 6, pp. 733−747, 2003.
[14] F. Yamazaki, K. Kouchi, and M. Matsuoka, "Tsunami damage detection using moderate-resolutuion satellite imagery," *Proceeding of the 8th U.S. National Conference on Earthquake Engineering*, California, US, 2006.
[15] M. Papathoma, D. Dominey-Howes, Y. Zong, and D. Smith, "Assessing tsunami vulnerability, an example from Herakleio, Crete," *Nat. Hazards Earth Syst. Sci*., vol. 3, pp. 377−389, 2013.
[16] F. Dall'Osso, M. Gonella, G. Gabbianelli, G. Withycombe, and D. Dominey-Howes, "A revised (PTVA) model for assessing the vulnerability of buildings to tsunami damage," *Nat. Hazards Earth Syst. Sci.*, vol. 9, pp. 1557−1565, doi:10.5194/nhess-9-1557-2009, 2009.
[17] F. Dall'Osso, L. Bovio, A. Cavalletti, F. Immordino, M. Gonella, and G. Gabbianelli, "A novel approach (the CRATER method) for assessing tsunamivulnerability at the regional scale using ASTER imagery," *Italian Journal of Remote Sensing*, vol. 42, no. 2, pp. 55−74, 2010.
[18] B. Horn, "Hill shading and the reflectance map," *Proceedings of IEEE*, vol. 69, no. 1, 1981, pp. 14−47.

[19] K. Iida, "Magnitude, energy and generation mechanisms of tsunamis and a catalogue of earthquakes associated with tsunamis," *Proceeding of Tsunami Meeting at the 10th Pacific Science Congress*, 1963, pp. 7−18.
[20] R. A. Van Zuidam, *Guide to Geomorphologic−Aerial Photographic Interpretation and Mapping,* International Institute for Geo-Information Science and Earth Observation, Enschede, The Netherlands, 1983.
[21] A. R. Huete, "A Soil-Adjusted Vegetation Index (SAVI)," *Remote Sensing of Environment*, vol. 25, no.3, pp. 295−309, 1988.
[22] L. S. Araujo, Joao Roberto dos Santos, Yosio Edemir Shimabukuro, "Relationship between SAVI and biomass data of forest and savanna contact zone and the Brazilian Amazonia," *International Archives of Photogrammetry and Remote Sensing*, vol. XXXIII, part B7, Amsterdam, 2000.
[23] M. Bouvet, G. Chander, P. Goryl P, R. Santer, Saunier, "Preliminary radiometric calibration assessment of ALOS AVNIR-2," *Geoscience and Remote Sensing Symposium, IEEE International*, pp. 2673−2676, 23−28 July 2007.
[24] A. K. Sah, B. P. Sah, K. Honji, N. Kubo, S. Senthil, "Semi-automated cloud/shadow removal and land cover change detection using satellite imagery," *International Archives of the Photogrammetry, Remote Sensing and Spatial Information Sciences*, vol. XXXIX-B7, XXII ISPRS Congress, Melbourne, Australia, 25 August–01 September 2012, pp. 335−340.
[25] M. C. Hanse, R. S. Defries, J. R. G. Townshend, R. Sohlberg, "Global land cover classification at 1km spatial resolution using a classification tree approach," *International Journal of Remote Sensing*, vol. 21, pp. 1331−1364, 2000.
[26] P. Gong P, R. Pu, G. S. Biging, M. R. Larrieu, "Estimation of forest Leaf area index using vegetation indices derived from hyperion Hyperspectral data," *IEEE Transactions on Geoscience and Remote Sensing*, vol. 41, no. 6, 2003.
[27] A. R. Huete, "A Soil-Adjusted Vegetation Index (SAVI)," *Remote Sens. Environ.*, vol. 25, 295−309, 1988.
[28] J. R. Jensen, *Remote Sensing of the Environmental Earth Resources Perspective*, Prentice Hall, New Jersey-USA, 2000.
[29] J. Qi, A. Chehbouni, A. R. Huete, Y. H. Kerr, and S. Sorooshian, "A Modified Soil Adjusted Vegetation Index," *Remote Sens. Environ.*, vol. 48, pp. 119−126, 1994.
[30] T. L. Saaty, "A scaling method for priorities in hierarchical structures," *Journal of Mathematical Psychology*, vol. 15, pp. 234−281, 1977.
[31] T. L. Saaty, *The analytic hierarchy process, planning, priority setting, resource allocation*, McGraw-Hill, New York, 1980, pp. 287.
[32] T. L. Saaty, "Decision making with the AHP; why is the principle eigenvector necessary," *Eur J Oper Res*, vol. 145, 85–91, 2003.
[33] A. M. Youssef, B. Pradhan, E. Tarabees, "Integrated evaluation of urban development suitability based on remote sensing and GIS techniques: contribution from the analytic hierarchy process," *Arab J Geosci*, vol. 4, pp. 463–473, 2010.
[34] T.L Saaty, "Decision making for leaders: The analytical hierarchy process for decisions in a complex world," *The Analytical Hierarchy Process Series*, vol. 2, pp. 71−74, 1996.
[35] E. H. Forman, M. A. Selly, *Decision by Objectives*, World Scientific Publishing Company, 2001.
[36] J. R. Eastman, W. Jin, P. A. K. Kyem, J. Toledano, "Raster procedures for multi-criteria/multi-objective decisions," *Photogrammetric Engineering & Remote Sensing*, *American Society for Photogrammetry and Remote Sensing*, vol. 61, no. 5, pp. 539–547, 1995.
[37] Geospatial Authority of Japan (GSI), *Map of inundation area due to the 2011 Great East Japan Earthquake*, Map number 61, 62, 65, 66, 68, 69, 70, 71, available at www.gsi.go.jp/kikaku/kikaku40016.html., Accessed on 25 June 2013.